Meteorologische Zeitschrift, Vol. **21**, No. 1, 049-059 (February 2012)
© by Gebrüder Borntraeger 2012

Article

Ozone highs and associated flow features in the first half of the twentieth century in different data sets

STEFAN BRÖNNIMANN[1]* and GILBERT P. COMPO[2,3]

[1]Oeschger Centre and Institute of Geography, University of Bern, Switzerland
[2]Climate Diagnostics Center, CIRES, University of Colorado, Boulder, USA
[3]Physical Sciences Division, Earth System Research Laboratory, NOAA, Boulder, USA

(Manuscript received January 12, 2011; in revised form April 14, 2011; accepted April 29, 2011)

Abstract

In order to better understand weather extremes, their relation to the large-scale climate variability, and their possible changes over time, observation-based atmospheric data sets are required that reach back in time as far as possible and that provide information on the 3-dimensional structure of the atmosphere. A number of new such data sets have been published in recent years, including historical observations, reanalyses, and reconstructions, some of which reach back into the nineteenth century. However, their usefulness for studying weather extremes remains to be shown. Here we compare some of these historical data sets in the first half of the twentieth century, focusing on one specific type of extreme, namely "ozone highs". Using historical total ozone observations as a starting point, we assess dynamical links between total ozone, the flow near the tropopause, and tropospheric circulation in the "Twentieth Century Reanalysis" (20CR), historical radiosonde and aircraft observations, and hand drawn historical maps. Selected cases are presented for two regions (Europe and China). Ozone highs over Europe in the 1920s to 1950s were qualitatively well reproduced in 20CR and could mostly be interpreted in the context of cut-off lows. Some of these coincided with a blocking high over the North Atlantic or with vigorous cold-air outbreaks. One of these cases is analysed in more detail. Ozone highs over China in the 1930s may have been related to changes in the jet stream and the subtropical tropopause, but they were not always well reproduced in 20CR. The results demonstrate that, in many of the cases, the available data allow a dynamical interpretation. This confirms the potential of the available data and techniques to extend the length of atmospheric data sets suitable for studying extremes.

1 Introduction

Weather extremes are rare by definition and hence long data sets reaching back in time as far as possible are needed for analyzing their occurrence, their relation to the large-scale circulation and climate variability, and their possible changes over time. At the same time, dynamical interpretations of extremes require detailed knowledge of the vertical structure of the atmosphere (i.e., upper-level flow features such as blocking or jet streams). Therefore, until recently, the time frame available for such studies was limited to the last 50–60 years, i.e., the periods of ERA-40 (UPPALA et al., 2005) or NCEP/NCAR (KISTLER et al., 2001) reanalysis data.

During the last few years major attempts have been undertaken to extend observation-based upper-air data products back in time. In addition to compilations of upper-air (STICKLER et al., 2010) and total ozone (BRÖNNIMANN et al., 2003b) observations, a new reanalysis has been produced. The "Twentieth Century Reanalysis" (20CR, COMPO et al., 2011), which is constrained only at the surface, provides 6-hourly 3-dimensional global data back to 1871 using an ensemble assimilation approach (WHITAKER and HAMILL, 2002). The data set might be useful for studying extremes, but it has not yet been assessed. In this paper we analyse one specific aspect in these data sets, namely the variability and extremes in total ozone in the first half of the twentieth century. This is of interest as total ozone variations are associated with specific flow features that themselves may be relevant for extreme weather. The depiction of another type of extremes in 20CR, namely midlatitude storms, is addressed in another paper in this issue (BRÖNNIMANN et al., 2012)

In 1926, DOBSON and HARRISON (1926) found that total ozone is closely correlated with the altitude of the tropopause (see Figure 1). This being the era before radiosondes, they hoped that total ozone could provide useful upper-air information on an operational basis for weather forecasting (for a history of ozone research see MÜLLER, 2009). While Dobson's dream finally came true decades later, when satellite ozone data were assimilated into operational analyses to improve weather forecasts, we now use the total ozone data measured by Dobson and many others during these early years for analyzing atmospheric dynamics in historical times. Hence, we are using the total ozone observations for the very purpose they were made for. After describing the data sets (Section 2), we first compare the historical total ozone observations with total ozone and upper-level geopotential height (GPH) from 20CR (Section 3). Then we se-

*Corresponding author: Stefan Brönnimann, Oeschger Centre for Climate Change Research and Institute of Geography, University of Bern, Hallerstrasse 12, 3012 Bern, Switzerland

0941-2948/2012/0284 $ 4.95
DOI 10.1127/0941-2948/2012/0284
© Gebrüder Borntraeger, Stuttgart 2012

lect cases with extremely high total ozone values in the observations and analyse these situations in 20CR and other data sets (Section 4), focusing on two regions (Europe and China). Conclusions are drawn in Section 5.

2 Data

2.1 Total ozone data

One of the most important time lines in the history of total ozone observations (as well as radiosonde observations) is the International Geophysical Year (IGY) 1957/58, which led to improved, globally coordinated, standardized, and calibrated networks. For the time period after 1957, many data sets are available for total ozone (see World Ozone and Ultraviolet Radiation Data Center WOUDC) as well as for radiosonde observations and for upper-level circulation (e.g., ERA-40 reanalysis, UPPALA et al., 2005). The focus of this study is on the time period prior to the IGY for which not much information has previously been available. Therefore we selected all available total ozone series which have data prior to the IGY, but used those series up to 1963 in order to have a comparison across this important time line. We have used long historical total ozone data from Arosa, Switzerland (46.8° N, 9.7° E) (STAEHELIN et al., 1998) and Oxford, UK (51.8° N, 1.2° W) (VOGLER et al., 2007) as well as many short series (see BRÖNNIMANN et al., 2003b and VOGLER et al., 2006 for details). Note that we omitted all series whose precision was assessed as "poor" in BRÖNNIMANN et al. (2003b) as well as those with less than 150 days with observations. In total around 30 historical series were used (see Table 1). The historical total ozone observations are denoted TOZ_{hist} in the following. The focus in this study is on the series from Arosa (since 1926), which can be considered as a high-quality series, as well as a series from Zi-Ka-Wei (Shanghai), China (31.2° N, 121.4° E), 1932–1936 (BRÖNNIMANN et al., 2003b), which is at an interesting location near the position of the subtropical jet.

In order to compare the correlations found in historical times with those found in the present using state of the art data sets, we used the total ozone data set from New Zealand's National Institute of Water and Atmospheric Research (NIWA) from BODEKER et al. (2005) from 1997 to 2007. The data set (called TOZ_{NIWA} hereafter) is a blend of different satellite data sets that were merged based on comparisons with ground-based data. The period 1997–2007 was chosen because of the good data coverage and in order to avoid a possible effect of the Pinatubo eruption.

2.2 Reanalysis data

The main reanalysis data set used in this study is the Twentieth Century Reanalysis version 2 (20CR), which

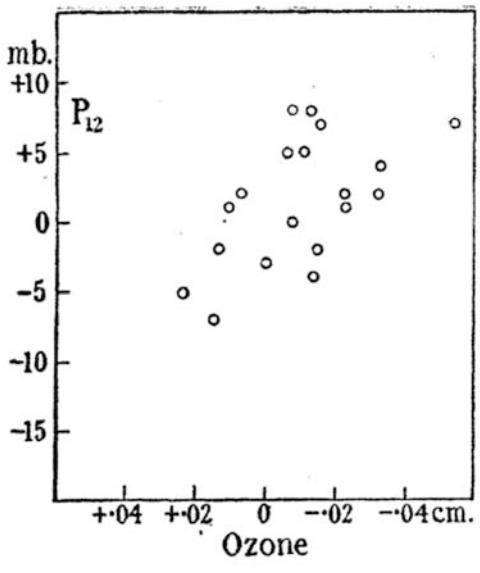

Figure 1: Scatter plot of anomalies (from a mean annual cycle) of total ozone and pressure at 12 km from balloon sounding data (from DOBSON and HARRISON, 1926).

is a global 3-dimensional atmospheric dataset reaching back to 1871. 20CR produces 6-hourly global analyses based on assimilation of surface and sea level pressure observations (COMPO et al. 2011). Monthly mean sea surface temperature and sea ice concentration from the HadISST dataset (RAYNER et al., 2003) are prescribed as boundary conditions Assimilation was performed using an Ensemble Kalman filter (EnKF) with first guess fields generated by a 2008 experimental version of the US National Centers for Environmental Prediction Global Forecast System atmosphere/land model (NCEP/GFS). The GFS was integrated at a resolution of T62 in the horizontal and 28 hybrid sigma-pressure levels in the vertical. The ensemble contained 56 ensemble members. Thus, in addition to the ensemble mean (which is mostly used in this paper), 20CR also provides a measure of uncertainty (the ensemble standard deviation). Details are given in COMPO et al. (2011).

We analyse fields of 200 hPa GPH ($Z200_{20CR}$) as well as temperature at various levels and tropopause wind speed. In addition to meteorological variables, 20CR also provides total ozone fields (denoted TOZ_{20CR} hereafter). The GFS model uses a prognostic ozone scheme and dynamically transports ozone throughout the first guess integration (SAHA et al., 2010). The climatological ozone production and loss terms in the scheme were computed with the Naval Research Laboratory (NRL) CHEM2D model (MCCORMACK et al., 2006), a two-dimensional (latitude-altitude) photochemical-transport model of the middle atmosphere, and are courtesy of NRL and NCEP. The calculations include the effects of gas-phase ozone loss due to chlorine compounds (in addition to many other species), and are representative of late 20$^{\text{th}}$ century stratospheric chlorine levels (J. MCCORMACK, pers. comm., 2011).

Table 1: Historical total ozone stations used in this study (see BRÖNNIMANN et al., 2003a). *n* denotes the number of days with observations within the period 1924–1963.

Station name	period	lon (° E)	lat (° N)	n
Aarhus	1952-1963	10.6	56.3	3462
Aldergrove	1952-1957	-6.2	54.7	1415
Arosa	1926-1963	9.7	46.8	7497
Bombay	1936-1938	72.9	18.9	402
Camborne	1952-1953	-5.3	50.2	3283
Canberra	1929-1932	149	-35.3	855
Christchurch	1928-1929	172.6	-43.5	231
College	1952-1957	-147.5	64.7	394
Dombas	1940-1946	9.1	62.1	1410
Edmonton	1950-1952	-113.5	53.6	557
Flagstaff	1954-1957	-111.7	35.2	463
Gulmarg	1955-1956	74.4	34.1	298
Helwan	1928-1929	31.3	29.9	182
Hemsby	1952-1955	1.7	52.7	855
Kodaikanal	1928-1929	77.5	10.2	191
Lerwick	1926-1963	-1.2	60.1	3462
Lindenberg	1926-1927	14.1	52.2	163
Magny	1955-1959	2.1	48.7	1054
Marseille	1927-1928	5.4	43.3	477
Mount Abu	1951-1960	72.7	24.6	2278
New Delhi	1955-1957	77.2	28.6	920
New York	1941-1944	-73.9	40.9	899
Oxford	1924-1963	-1.2	51.8	7053
Rome	1954-1963	12.2	42.1	3152
Spitsbergen	1950-1962	15	78	1676
Srinagar	1956-1957	74.8	34.1	182
Table Mountain	1928-1929	-117.3	34.1	354
Tateno	1955-1957	140.1	36.1	409
Uppsala	1952-1963	17.6	59.9	2472
Zi-Ka-Wei	1932-1936	121.43	31.2	637

The 20CR EnKF implementation does not increment the ozone field generated by the first guess, but the effect of observations is felt in the ozone field through the modified dynamical and thermodynamical fields after each 6-hourly analysis cycle.

For independent comparison with total ozone in the present time we have also used 6-hourly data on 200 hPa GPH from the ERA-Interim reanalysis ($Z200_{ERAINT}$, DEE et al., 2011). For some parts of the study, the reanalysis fields were bilinearly interpolated to the locations of observing stations.

2.3 Historical upper-air observations and hand drawn historical weather maps

In addition to analyzing total ozone observations and reanalysis data, we also analysed historical upper-air observations. We used temperature observations from radiosondes and aircraft from several sites in north eastern Europe, 1940, from BRÖNNIMANN (2003). These data are now part of the Comprehensive Historical Upper Air Network CHUAN (STICKLER et al., 2010).

A large amount of historical weather information for a given event is often accessible, though not in numerical form, as hand-drawn analysis maps. For the case studies presented in Section 4, we also consulted such weather maps. For Europe in the 1940s these were taken from the German Weather report (Täglicher Wetterbericht der Deutschen Seewarte). Similarly, for China we also used contemporary publications, which contained hand analyses of total ozone extremes and hand-drawn weather maps for eastern China for selected days in the 1930s (LEJAY, 1937).

3 Total ozone statistics

First, we analysed the mean annual cycle of TOZ_{hist} and TOZ_{20CR}, and then we compared the residuals and analysed their distribution. Results are shown in detail for two sites (Arosa and Zi-Ka-Wei) in Figure 2. Mean annual cycles were obtained by least-squares fitting of the first two harmonics of the day of year to the data (Figure 2 left). For both stations, the annual cycles of TOZ_{20CR} and TOZ_{hist} are very similar in shape, but the amplitude is somewhat smaller in TOZ_{20CR} than in TOZ_{hist}. There is an offset in the case of Zi-Ka-Wei which might be due to systematic errors in the observations (see also BRÖNNIMANN et al., 2003b).

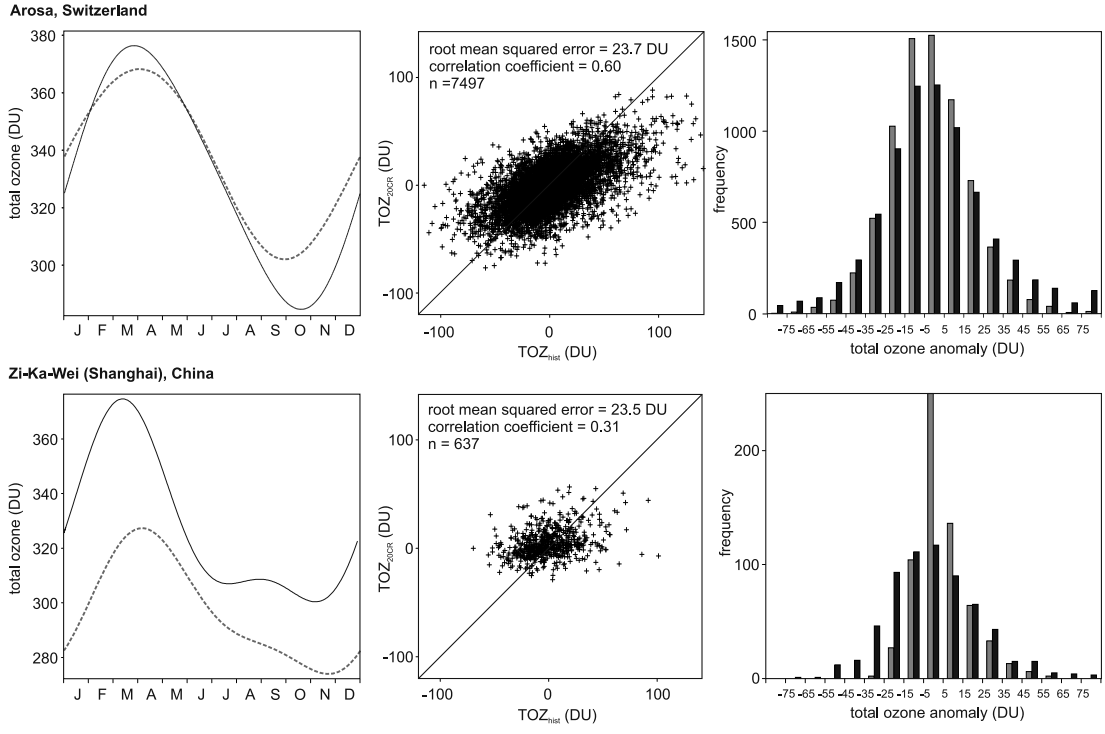

Figure 2: Comparison between TOZ_{hist} (thin black) and TOZ_{20CR} (thick grey dashed) for total ozone at Arosa, Switzerland, 1924–1963 (top) and Zi-Ka-Wei (Shanghai), China, 1932–1936 (bottom). (left) Mean annual cycle (obtained by extracting the first two harmonics and the time mean). (middle) Scatter plot of anomalies from the mean annual cycle (number of points, correlation coefficient, and root mean squared error are given). (right) Histograms of the anomalies for TOZ_{hist} (black) and TOZ_{20CR} (grey).

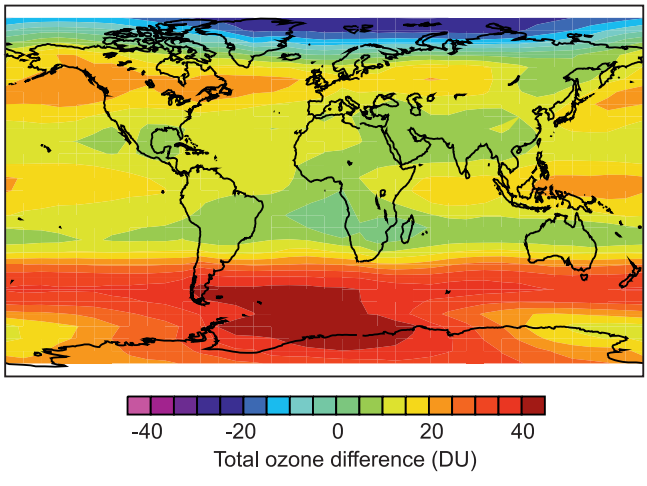

Figure 3: Difference between TOZ_{20CR} and TOZ_{NIWA} averaged for 1997–2007.

The middle panel of Figure 2 shows scatterplots of the anomalies from the mean annual cycles for TOZ_{hist} and TOZ_{20CR}. For Arosa a good overall agreement is found (correlation of 0.6). The relation clearly deviates from the 1:1 line. To some extent this is expected as 20CR is an ensemble product and hence extremes are expected to be smoothed out in the absence of observations to increment the analysis. However, as will be shown in Section 4, the magnitude of extreme anomalies is underestimated even if this effect is taken into account. The correlation coefficient is much weaker (0.31) for Zi-Ka-Wei, though also highly significant (99 % significance level assuming 70 degrees of freedom, with $n = 637$ but high first order serial correlation of 0.5 to 0.8). Specifically, it becomes visually apparent that extremes in the observations are not very well captured in 20CR.

The histograms of the anomalies are shown in the right panel. Again, we expect less dispersion in TOZ_{20CR} compared to TOZ_{hist} due to the ensemble averaging, as is seen in the case of Arosa. The standard deviation is smaller in TOZ_{20CR} anomalies (20.9 DU) compared to TOZ_{hist} anomalies (29.3 DU). For Zi-Ka-Wei we find an asymmetric difference between the histograms from the two sources. Moderate to strong negative anomalies are even more infrequent in TOZ_{20CR} compared to TOZ_{hist} than moderate to strong positive anomalies. Zi-Ka-Wei is located close to the latitude with the strongest meridional gradient in total ozone (i.e., between the tropical and extratropical tropopause). Strong negative total ozone anomalies in this region occur most often in winter due to intrusion of tropical air masses. Small biases in the depiction of this climatological gradient may have a large effect on total ozone in 20CR. Furthermore, exchange processes between the troposphere and stratosphere that affect ozone may occur near the subtropical jet with a relatively fine structure, which might be insufficiently resolved in 20CR

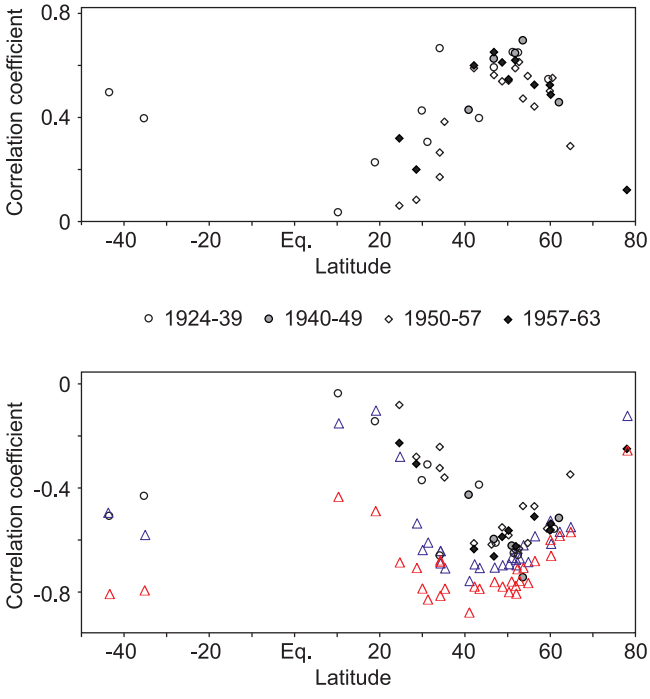

Figure 4: Anomaly correlations between TOZ_{hist} and TOZ_{20CR} (top, positive correlations), and TOZ_{hist} and $Z200_{20CR}$ (bottom, negative correlations) as a function of latitude and time period. Open circles, grey filled circles, open diamonds, and filled diamonds refer to the time periods 1924–1939, 1940–1949, 1950-1957, and 1957–1963, respectively. The red and blue triangles in the bottom plot show the anomaly correlations for the same locations between $Z200_{20CR}$ and TOZ_{20CR} (1924–1963) and between $Z200_{ERAINT}$ and TOZ_{NIWA} (1997–2007), respectively (see Table 1 for a station list).

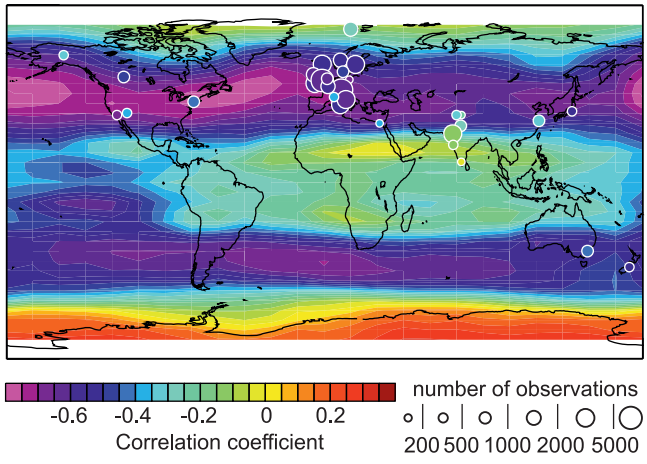

Figure 5: Anomaly correlations between $Z200_{20CR}$ and $Z200_{TOZ}$ (1924–1963, circles) and between $Z200_{ERAINT}$ and TOZ_{NIWA} (1997–2007, contours). The size of the circle indicates the number of observations for the stations listed in Table 1.

(e.g., WAUGH, 2005; PAN et al., 2009).

In order to address the bias issues raised in Figure 2, we compared TOZ_{20CR} with TOZ_{NIWA} in the 1997–2007 period (see Figure 3). North of about 40° S, deviations are within ±25 DU, i.e., within a few percent. Larger deviations are found in the southern high latitudes, where 20CR underestimates the depth and area of the ozone hole. The correlation between independent historical ozone observations and 20CR is studied in Figure 4. We show, as a function of time period and latitude, the correlations for all stations between TOZ_{20CR} and TOZ_{hist} (Figure 4 top) as well as correlations between $Z200_{20CR}$ and TOZ_{hist} (Figure 4 bottom). The limitation of the analysis to series with $n > 150$ allows some comparability between the correlations. The chosen time periods reflect major phases in instrument and network development such as photographic detection (1924–1939), photoelectric detection (1940–1949), the use of photomultipliers (1950–1957) and the use of a double wave-length pair (1957–1963, see BRÖNNIMANN et al. (2003a), for details). Correlations are generally strong in the northern midlatitudes and decrease towards the pole and the tropics. No clear differences are found as a function of time period. This is also true for the period 1957–1963, when the data quality in the total ozone network was substantially improved. In general the correlations fit very well with those found in previous studies (BRÖNNIMANN et al., 2003b; VOGLER et al., 2007) for correlations between anomalies of observed total ozone and historical upper-air data.

Changes in the flow near the tropopause are the dominant cause for day-to-day variability in total ozone at midlatitudes (VAUGHAN and PRICE, 1991). This explains the strong negative correlations between $Z200_{20CR}$ and TOZ_{hist}. The correlation between TOZ_{20CR} and TOZ_{hist} is very similar to that between $Z200_{20CR}$ TOZ_{hist} (but with the sign reversed). This suggests that most of the changes produced by the ozone scheme in 20CR result from changes in the flow near the tropopause. In tropical and polar regions, in the real atmosphere, total ozone variability is smaller and other processes (both dynamical and chemical) may gain more weight (for a general overview see WMO/UNEP, 2010). These processes may not be captured in 20CR.

To further study this point, we also correlated $Z200_{20CR}$ and TOZ_{20CR} (over the entire period 1924–1963, red symbols) and performed the same analysis using $Z200_{ERAINT}$ and TOZ_{NIWA} for the 1997–2007 period (blue symbols). Of all data sets studied in this paper, the latter comparison arguably is closest to the real atmosphere and is here considered as a reference. As mentioned above, correlations are strongest at midlatitudes and weaker in the tropics and the polar regions. The correlation of TOZ_{hist} with $Z200_{20CR}$ does not deviate very strongly from the reference except near 30° N. The correlation between TOZ_{20CR} and $Z200_{20CR}$, however, is much stronger than in the reference, possibly because other processes that would affect ozone variability are less well represented in 20CR.

The lack of agreement in the correlations near 30° N is not surprising as this is near the location of the

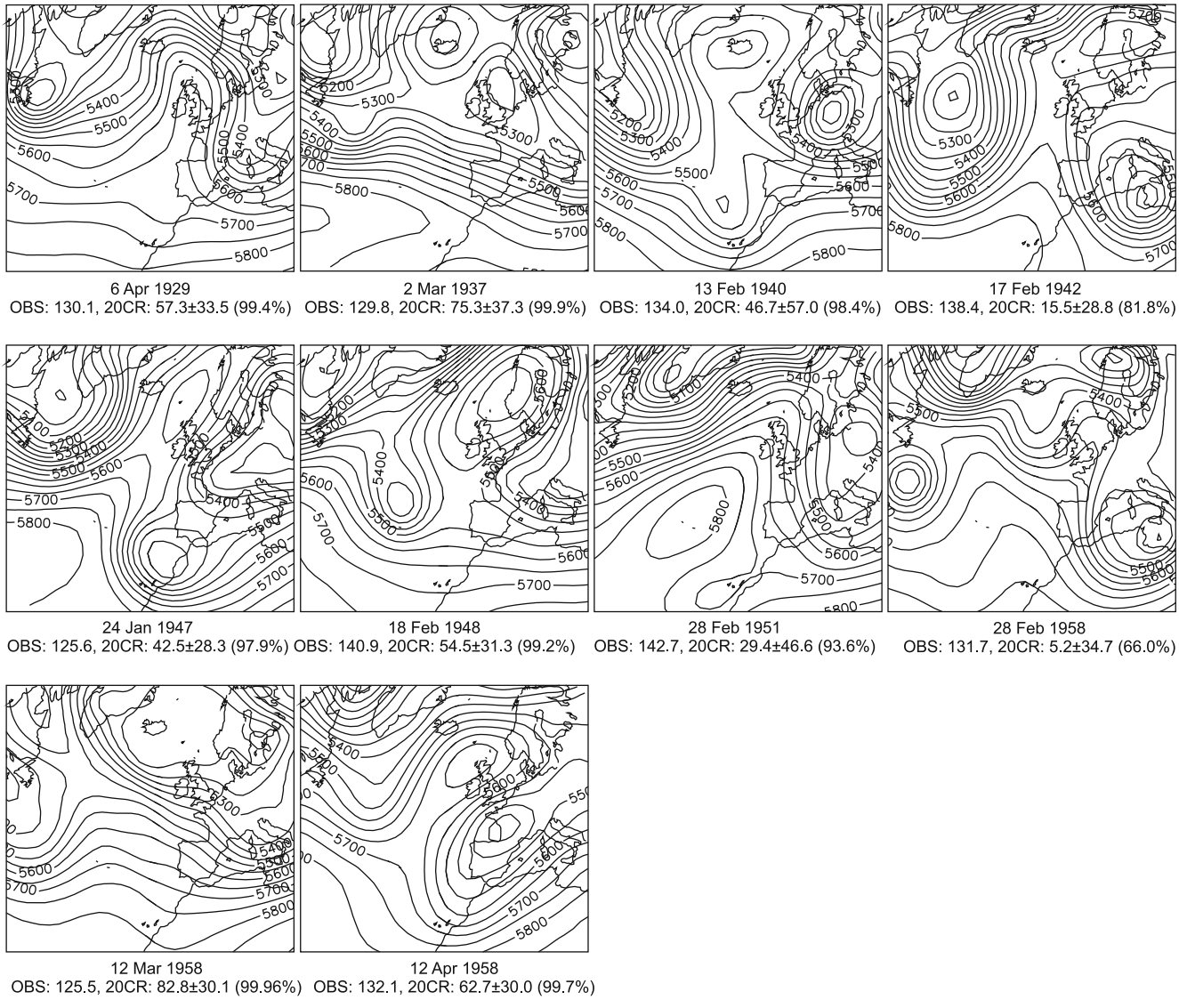

Figure 6: 500 hPa GPH (in gpm) over the North Atlantic-European sector from 20CR for the 10 days with highest observed total ozone anomalies at Arosa in the period 1924–1963. Numbers below the figure give total ozone anomalies (in DU) in observations and in 20CR (± 2 standard deviations of the ensemble spread) as well as the corresponding percentile value for 20CR (in brackets).

strongest gradient in the total ozone field. However, to further investigate this point we plotted the full spatial structure of the correlation between total ozone and 200 hPa GPH (Figure 5). The analysis of the reference (i.e., $Z200_{ERAINT}$ correlated with TOZ_{NIWA} for 1997–2007) shows that there are clear longitudinal differences. Correlations between TOZ_{NIWA} and $Z200_{ERAINT}$ are particularly low in the monsoon regions. The same pattern is found in the historical period, but the correlations are even lower. Otherwise we find a good qualitative agreement of the spatial structure.

In all, the correlations are somewhat worse in the historical period which may be due to errors and uncertainties in both the historical total ozone data and 20CR (BRÖNNIMANN et al., 2003b). Also, some of the series are relatively short. The only region with consistently lower correlations in the historical period is India; again, errors and uncertainties in both the historical total ozone data and 20CR might be the cause. In light of these issues, the agreement is promising and shows that obtaining dynamical information from the tropopause region for specific events in the 1930s and 1940s might be possible.

4 Dynamical analysis of "ozone highs"

4.1 Europe

From the two series of Arosa and Zi-Ka-Wei, we selected the events with the highest observed total ozone anomalies for further investigation. For the case of Arosa we selected the 10 highest total ozone anomalies in the observed record (note that there are gaps in

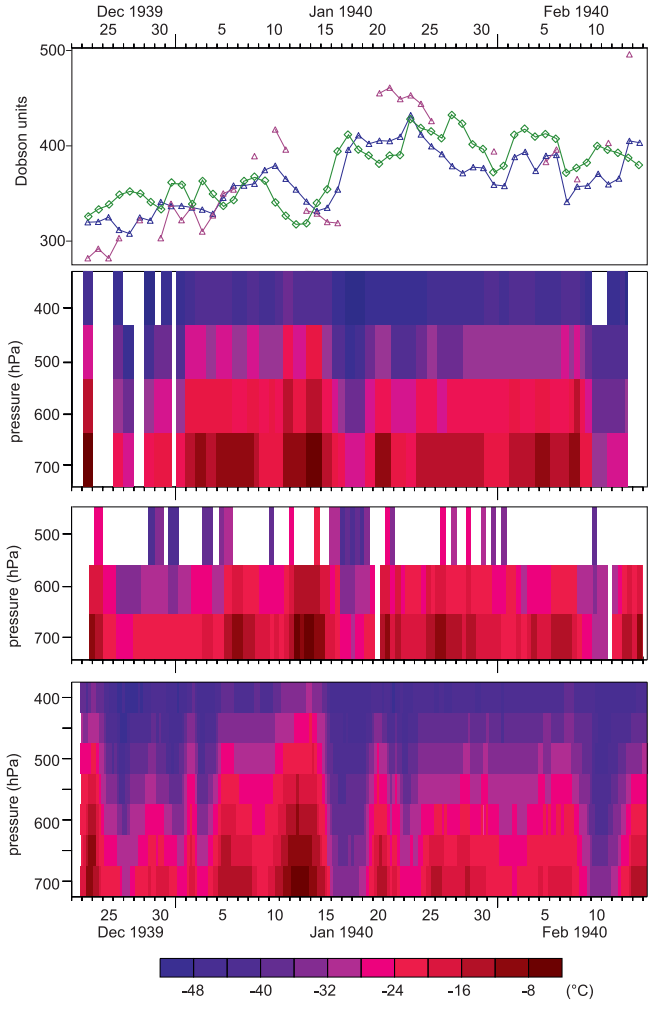

Figure 7: Time-height cross-sections of temperature in the Baltic region in the middle troposphere in December 1939 to February 1940 as well as total ozone at Arosa. (top) TOZ_{hist} (purple) and TOZ_{20CR} (blue) for Arosa as well as TOZ_{20CR} for the grid point [18°E, 56°N] (green). (middle) Time-height cross-sections of temperature from daily to twice daily radiosonde data from Swinoujscie (Poland), from twice daily aircraft ascents from Kaliningrad (Russia) and from 4-times daily data from 20CR (bottom) for the grid point [18°E, 56°N]. See Figure 8 for locations.

the series, i.e., higher values may have occurred), corresponding to values higher than the 99.85 percentile. All of them were also higher than the 60-percentile in TOZ_{20CR} anomalies, 8 out of the 10 were in the uppermost 10 % and 5 out of 10 were in the top 1 %. However, the amount of the anomaly is underestimated in 20CR even when taking the ensemble spread into account. Even if we assume an extreme observation uncertainty of 50 DU (assumed as an overestimation, since we select the highest cases), TOZ_{20CR} anomalies lie below TOZ_{hist} anomalies in half of the cases. Hence, most of these cases are qualitatively very well reproduced in the ensemble mean of the reanalysis, but not quantitatively.

Figure 6 shows the 500 hPa GPH field over the North Atlantic-European sector for these 10 days. Most of the cases are characterized by a cut-off low over Central Europe, in all other cases there is at least a strong trough. Cut-off lows are a type of blocking pattern, they usually develop from troughs, but then are displaced from the main westerly flow. Cut-off lows in the European region are most frequent in summer (for an overview and climatology see NIETO et al., 2007, 2008), but extreme ozone maxima occur more often in winter and spring. In this season, cut-off lows can be accompanied by blocking anticyclones. In fact, this is seen in several of the cases in Figure 6. Some events shown in Figure 6 exhibit a typical "omega" block (a west-to-east sequence of low-high-low; e.g., 13 Feb 1940, and 17 Feb 1942).

The lower stratospheric column is larger over cut off lows and troughs (where the tropopause is low). As a consequence, high total ozone is found. During the development of cut-off lows, stratospheric air may intrude into the troposphere in the form of narrow, elongated streamers (APPENZELLER and DAVIES, 1992). Relatively large variability in total ozone may therefore occur on spatial scales below the resolution of 20CR. Low amounts of total ozone may by associated with blocking high-pressure systems, although so-called "ozone mini holes" mostly result from a coupling of the blocking pattern with the polar vortex dynamics (BARRIOPEDRO et al., 2010). As a consequence, atmospheric blocking patterns as well as the Atlantic storm track leave a very clear signature in total ozone (ORSOLINI et al., 1998; ORSOLINI and DOBLAS-REYES, 2003).

Many of the cases shown in Figure 6 were accompanied by vigorous cold-air outbreaks (see also the additional cases of total ozone spikes associated with cold-air outbreaks in 1940–1942 studied in BRÖNNIMANN et al., 2004 based on observations). In the following we focus on a series of cold-air outbreaks in the winter 1939/1940, which we analyse in time-height cross-section of temperature in the middle to upper troposphere (Figure 7). The available upper-air observations (daily to twice-daily radiosonde data from Swinoujscie, from twice daily aircraft ascent from Kaliningrad) allow a detailed comparison with corresponding temperatures in 20CR and with total ozone information from both historical observations (Arosa) and 20CR.

The agreement between the temperature cross-sections in observations and 20CR is excellent, showing that even abrupt coolings of 20–25 °C in the free troposphere within two or three days are captured qualitatively and quantitatively in an ensemble data assimilation approach, whose synoptic and day-to-day variability is driven only by surface pressure. Moreover, 20CR shows relatively subtle details of the time evolution of the cold-air outbreaks. Many cold air outbreaks are associated with the total ozone spikes in Arosa. They do not occur simultaneously, which is probably due to the considerable distance (around 1000 km). TOZ_{20CR} for the nearby grid point shows a better alignment of ozone spikes with cold-air outbreaks (note also the agreement

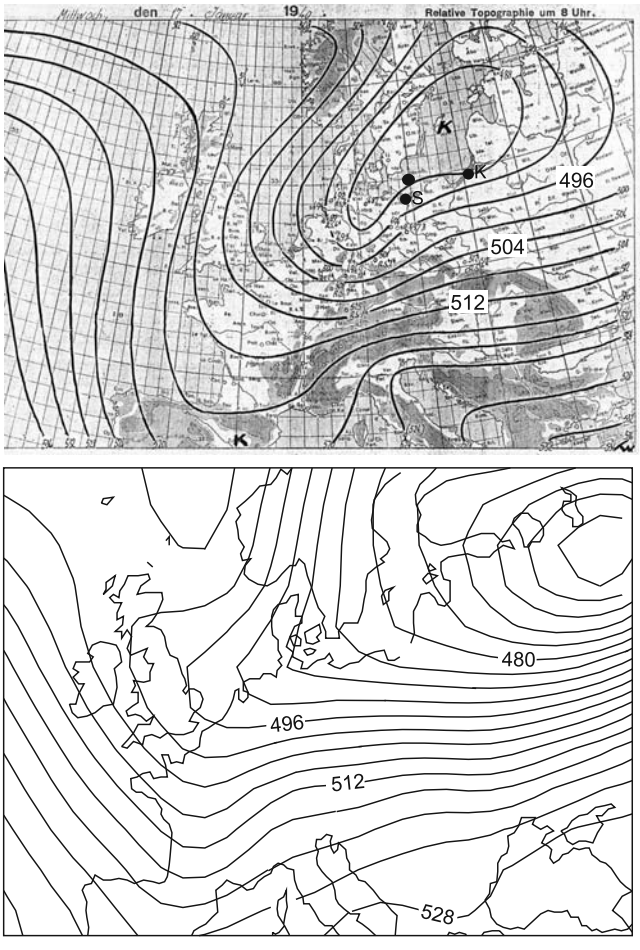

Figure 8: (top) Thickness between 1000 and 500 hPa (in geodynamic meters) over Europe on 17 January 1940, 8 CET from the German Weather Report. (bottom) same from 20CR, 17 January 1940, 6 UTC (note that the unit here also is geodynamic meters). The dots mark the locations of Swinoujscie (S), Kaliningrad (K) and the grid point used for the cross-section of 20CR in Figure 7.

of total ozone spikes in Arosa with cold-air outbreaks in a radiosonde record that is much closer to Arosa (see BRÖNNIMANN et al., 2004).

The scale of the cold-air outbreak is depicted in Figure 8, which shows the thickness between 500 and 1000 hPa on 17 Jan 1940. Both in the hand drawn maps from the German weather report (Figure 8, top) and in 20CR (bottom) the centre of the cold air was over the Baltic region and was extending to the southwest. There are some differences between the maps. It should be noted, however, that the hand drawn map is based only on ascents from central Europe. Hence the differences do not indicate disagreement.

Based on the comparisons in this section, 20CR is considered suitable for analyzing extreme total ozone events and accompanying flow features such as cut-off lows and cold-air outbreaks over the Atlantic-European region. It should be noted, however, that all of these analyses were based on the ensemble mean.

4.2 China

In the case of Zi-Ka-Wei, rather than performing our own selection, we used the selection of eight high-ozone days by LEJAY (1937) in the period 1934–1936. For these days (as well as for four low-ozone days), LEJAY (1937) provides daily weather maps with sea-level pressure and surface winds over East Asia. These fields can now be compared with 20CR. Of the eight high-ozone days, only four were reproduced by 20CR (the others had near-zero or negative anomalies). Here we show two typical examples; one case that was well reproduced and another that was not well reproduced. At the surface the general pressure distribution as well as the strong winter monsoon flow seen in the hand-drawn maps (Figure 9, left) are reproduced in 20CR (right). In particular, the storm on 26 Jan 1936 near Japan or other low pressure features are well captured (although the storm is shifted in longitude). This general tendency is also true for the other cases (not shown). However, the structure of the high pressure systems over China agrees less well, which may be due to errors in either or both, the hand drawn maps and 20CR. The ensemble spread in both cases is low (around 1 hPa) over the ocean but increases over mainland China and reaches several hPa. This is not surprising because, aside from Hong Kong, there are no surface or sea level pressure observations in the International Surface Pressure Databank version 2 over mainland China during this time period (not shown).

The top row (26 Jan 1934) is the case in which also the total ozone anomaly is reproduced. Zi-Ka-Wei is normally located close to the subtropical jet, which marks the boundary between the tropical and extratropical tropopause. Tropopause height (not shown) and total ozone also exhibit very strong gradients across this boundary (Figure 9, right). Note that we use the maximum of the wind speed at the tropopause to describe the location of the jet and of the gap between the tropical and extratropical tropopause. This procedure gives a simple measure of location, but does not allow distinguishing between misrepresentations of the jet position, of the altitude of the tropopause, or of small scale flow features which may not be adequately captured.

On 26 Jan 1934 the jet had a slightly more meridional orientation and was shifted equatorward from its normal position over Eastern China. The same was true for tropopause height and total ozone. Zi-Ka-Wei was to the north of the jet core, where the tropopause was much lower and total ozone much higher. On 26 Jan 1936, in contrast, the jet (which was stronger than in the previous case) was located to the north of or over Zi-Ka-Wei in 20CR, which therefore experienced more tropical total ozone values. The observations, on the other hand, point to a strong positive total ozone anomaly which is not in agreement with this situation. Further studies are needed to address possible problems in 20CR in this respect and whether additional surface and sea level pressure observations in this region could remedy them.

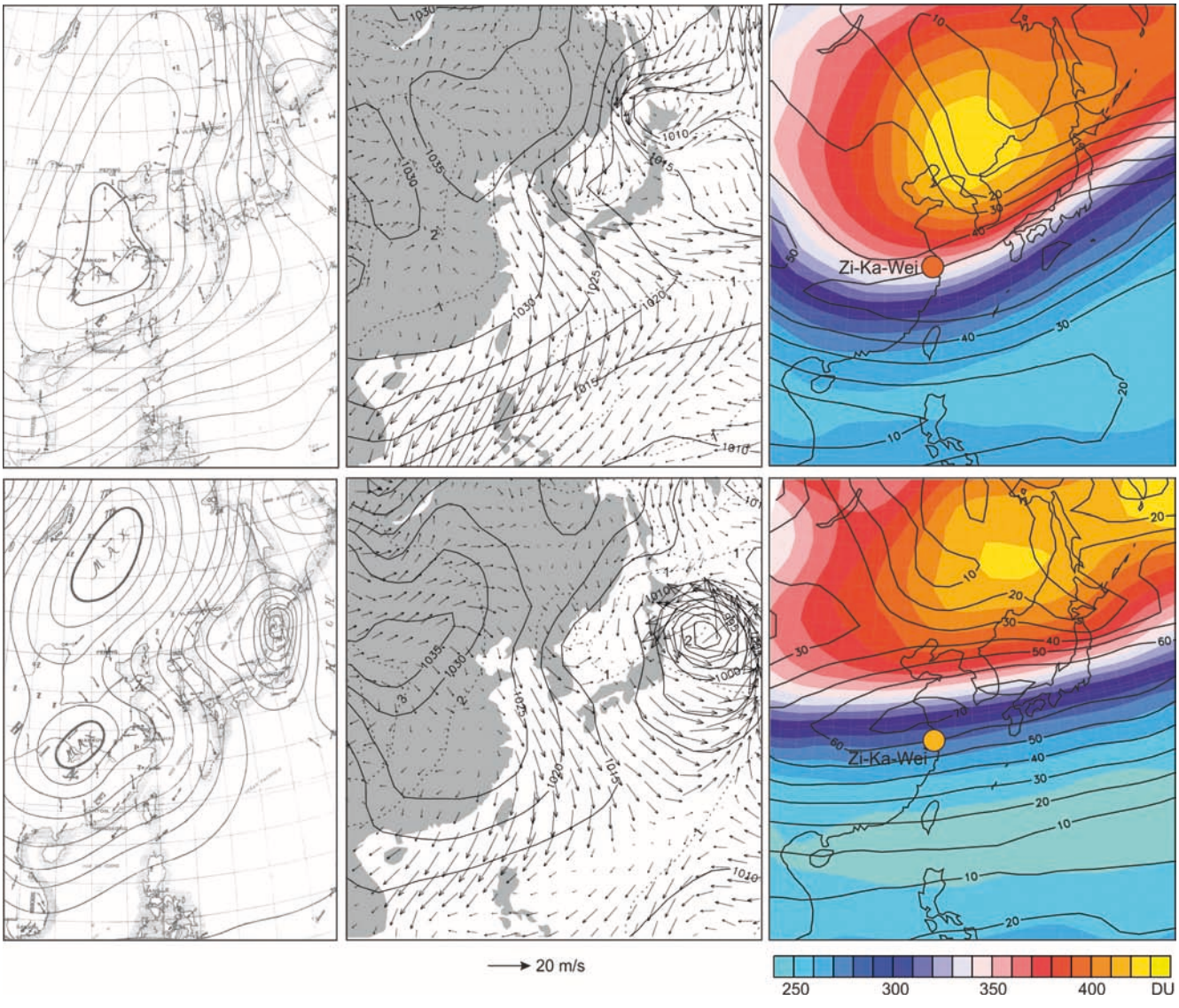

Figure 9: Meteorological fields for two cases (top: 26 January 1934, bottom: 26 January 1936) with high observed total ozone at Zi-Ka-Wei, China, in the 1930s. (left) Hand drawn historical weather chart with sea-level pressure (mm Hg) and wind vectors, (middle) sea-level pressure (solid contours, hPa), ensemble spread (standard deviation) of sea-level pressure (dotted contours, hPa), and winds at the 0.995 sigma level in 20CR, (right) total ozone (colours) and wind speed at the tropopause level (contours, in m/s) from 20CR. The coloured circles indicate the observed total ozone values.

Upper-air data from that region and time period are currently digitized and may help to further shed light on the problem.

5 Conclusions

In this paper we have compared several historical data sets, including the "Twentieth Century Reanalysis" (20CR) in the first half of the twentieth century, focusing on variability and extremes in total ozone and associated flow features. The statistical analysis of historical total ozone observations and upper-level variables in 20CR reproduces the expected maximum of correlations in the midlatitude storm track regions. The decrease of the correlation towards the tropics and polar regions is similar to modern data sets.

Individual extreme events ("ozone highs" that were often accompanied by cold-air outbreaks in the troposphere) were analysed for Europe and China. While there is relatively good agreement between 20CR and recent and historical total ozone observations in terms of the spatial patterns of variability, we note that 20CR underestimates the variability. Further, there are specific regions that need additional consideration. Still, it may come as a surprise that the 20CR is capable of even qualitatively capturing extreme total ozone events and their associated flow features in the Atlantic-European sector in the first half of the twentieth century.

Acknowledgments

Productive conversations are acknowledged with colleagues at NOAA/ESRL, J.S. WHITAKER and P.D. SARDESHMUKH (also of the University of Colorado CIRES Climate Diagnostics Center). Assistance with the NCEP GFS ozone parameterization was kindly provided by S. MOORTHI and S. SAHA at NCEP/Environmental Modeling Center and J. MCCORMACK of Space Science Division, Naval Research Laboratory. This work was funded by the Swiss National Science Foundation project EVALUATE. G. COMPO received support from the NOAA Climate Program and the Office of Science (BER), U.S. Department of Energy. 20CR data were obtained courtesy of the NOAA/OAR/ESRL PSD, Boulder, Colorado, USA, from their Web site at www.esrl.noaa.gov/psd/. Support for the Twentieth Century Reanalysis Project dataset is provided by the U.S. Department of Energy, Office of Science Innovative and Novel Computational Impact on Theory and Experiment (DOE INCITE) program, and Office of Biological and Environmental Research (BER), and by the NOAA Climate Goal. The Project used resources of the National Energy Research Scientific Computing Center and of the National Center for Computational Sciences at Oak Ridge National Laboratory, which are supported by the Office of Science of the U.S. Department of Energy under Contract No. DE-AC02-05CH11231 and Contract No. DE-AC05-00OR22725, respectively.

References

APPENZELLER, C., H.C. DAVIES, 1992: Structure of stratospheric intrusions in the troposphere. – Nature **358**, 570–572.

BARRIOPEDRO, D., M. ANTÓN, J.A. GARCÍA, 2010: Atmospheric blocking signatures in total ozone and ozone miniholes. – J. Climate **23**, 3967–3983.

BODEKER, G.E., H. SHIONA, H. ESKES, 2005: Indicators of Antarctic ozone depletion. – Atmos. Chem. Phys. **5**, 2603–2615.

BRÖNNIMANN, S. 2003: A historical upper-air data set for the 1939–1944 period. – Int. J. Climatol. **23**, 769–791.

BRÖNNIMANN S., J. STAEHELIN, S.F.G. FARMER, J.C. CAIN, T.M. SVENDBY T. SVENØE, 2003a: Total ozone observations prior to the IGY. I: A history. – Quart. J. Roy. Meteor. Soc. **129**, 2797–2817.

BRÖNNIMANN S., J.C. CAIN, J. STAEHELIN, S.F.G. FARMER, 2003b: Total ozone observations prior to the IGY. II: Data and quality. – Quart. J. Roy. Meteor. Soc. **129**, 2819–2843.

BRÖNNIMANN, S., J. LUTERBACHER, J. STAEHELIN, T.M. SVENDBY, 2004: An extreme anomaly in stratospheric ozone over Europe in 1940–1942. – Geophys. Res. Lett. **31**, L08101, DOI: 10.1029/2004GL019611.

BRÖNNIMANN, S., O. MARTIUS, H. VON WALDOW, C. WELKER, J. LUTERBACHER, G.P. COMPO, P.D. SARDESHMUKH, T. USBECK, 2012: Extreme winds at northern mid-latitudes since 1871. – Meteorol. Z. **21**, 13–27.

COMPO, G.P. and co-authors, 2011: The Twentieth Century Reanalysis Project. – Quart. J. Roy. Meteor. Soc. **137**, 1–28.

DEE, D.P., S.M. UPPALA, A.J. SIMMONS, P. BERRISFORD, P. POLI, S. KOBAYASHI, U. ANDRAE, M. A. BALMASEDA, G. BALSAMO, P. BAUER, P. BECHTOLD, A.C.M. BELJAARS, L. VAN DE BERG, J. BIDLOT, N. BORMANN, C. DELSOL, R. DRAGANI, M. FUENTES, A. J. GEER, L. HAIMBERGER, S.B. HEALY, H. HERSBACH, E.V. HÓLM, L. ISAKSEN, P. KÅLLBERG, M. KÖHLER, M. MATRICARDI, A.P. MCNALLY, B.M. MONGE-SANZ, J.-J. MORCRETTE, B.-K.PARK, C. PEUBEY, P. DE ROSNAY, C. TAVOLATO, J.-N.THÉPAUT, F. VITART, 2011: The ERA-Interim reanalysis: configuration and performance of the data assimilation system. – Quart. J. Roy. Meteor. Soc. **137**, 553–597.

DOBSON, G.M.B., D.N. HARRISON, 1926: Observations of the amount of ozone in the Earth's atmosphere and its relation to other geophysical conditions. – Proc. R. Soc. A **110**, 660–693.

KISTLER, R. and co-authors, 2001: The NCEP-NCAR 50-year reanalysis: monthly means CD-ROM and documentation. – Bull. Amer. Meteor. Soc. **82**, 247–267.

LEJAY, P., 1937: Mesures de la quantité d'ozone contenue dans l'atmosphère a observatoire do Zô-sé. - Notes de Meteorologie Physique (Observatoire de Zi-Ka-Wei), Fasc. VII, Shanghai.

MCCORMACK, J.P., S.D., ECKERMANN, D.E. SISKIND, T. MCGEE, 2006: CHEM2D-OPP: A new linearized gas phase photochemistry parameterization for high altitude NWP and climate models. – Atmos. Chem. Phys. **6**, 4943–4972.

MÜLLER, R., 2009: A brief history of stratospheric ozone research. – Meteorol. Z. **18**, 3-24

NIETO R., L. GIMENO, L. DE LA TORRE, P. RIBERA, D. BARRIOPEDRO, R. GARCIA-HERRERA, A. SERRANO, A. GORDILLO, A. REDAÑO, J. LORENTE, 2007: Interannual variability of cut-off low systems over the European sector: the role of blocking and the northern hemisphere circulation modes. – Meteor. Atmos. Phys. **96**, 85–101.

NIETO R., M. SPRENGER, H. WERNIL, R. TRIGO, L. GIMENO, 2008: Identification and climatology of cutoff lows near the tropopause. – Ann. New York Academy Sci. **1146**, 256–290.

ORSOLINI, Y. J., F. J. DOBLAS-REYES, 2003: Ozone signatures of climate patterns over the Euro-Atlantic sector in the spring. - Quart. J. Roy. Meteor. Soc. **129**, 3251–3263.

ORSOLINI, Y.J., D.B. STEPHENSON, F.J. DOBLAS-REYES, 1998: Storm tracks signature in total ozone during Northern Hemisphere winter. – Geophys. Res. Lett. **25**, 2413–2416.

PAN, L. L., W.J. RANDEL, J C. GILLE, W.D. HALL, B. NARDI, S. MASSIE, V. YUDIN, R. KHOSRAVI, P. KONOPKA, D. TARASICK, 2009: Tropospheric intrusions associated with the secondary tropopause. – J. Geophys. Res. **114**, D10302, DOI:10.1029/2008JD011374.

RAYNER, N., D.E. PARKER, E.B. HORTON, C.K. FOLLAND, L.V. ALEXANDER, D.P. ROWELL, E.C. KENT, A. KAPLAN, 2003: Global analyses of sea surface temperature, sea ice, and night marine air temperature since the late nineteenth century. - J. Geophys. Res. 108(D14), 4407, doi:10.1029/2002JD002670.

RIEDER, H. E., J. STAEHELIN, J. MAEDER, T. PETER, M. RIBATET, A. C. DAVISON, R. STÜBI, P. WEIHS, F. HOLAWE, 2010: Extreme events in total ozone over Arosa – Part 1: Application of extreme value theory. – Atmos. Chem. Phys. **10**, 10021–10031.

SAHA, S. and co-authors, 2010: The NCEP Climate Forecast System Reanalysis. – Bull. Amer. Meteor. Soc. **91**, 1015–1057.

STAEHELIN J., A. RENAUD, J. BADER, R. MCPETERS, P. VIATTE, B. HOEGGER, V. BUIGNON, M. GIROUD, H. SCHILL, 1998: Total ozone series at Arosa (Switzerland): Homogenisation and data comparison. – J. Geophys. Res. **103**, 5827–5841.

STICKLER, A. and co-authors, 2010: The Comprehensive Historical Upper Air Network (CHUAN). – Bull. Amer. Meteor. Soc. **91**, 741–751.

UPPALA, S. M., and co-authors, 2005: The ERA-40 reanalysis. – Quart. J. Roy. Meteor. Soc. **131**, 2961–3012.

VAUGHAN, G., J.D. PRICE, 1991: On the relation between total ozone and meteorology. – Quart. J. Roy. Meteor. Soc. **117**, 1281–1298.

VOGLER, C., S. BRÖNNIMANN, G. HANSEN, 2006: Re-evaluation of the 1950–1962 total ozone record from Longyearbyen, Svalbard. – Atmos. Chem. Phys. 6, 4763-4773.

VOGLER, C., S. BRÖNNIMANN, J. STAEHELIN, R.E.M. GRIFFIN, 2007: The Dobson total ozone series of Oxford: Re-evaluation and applications. – J. Geophys. Res. **112**, D20116.

WAUGH, D.W., 2005: Impact of potential vorticity intrusions on subtropical upper tropospheric humidity. – J. Geophys. Res. **110**, D11305, DOI:10.1029/2004JD005664.

WHITAKER, J. S., T.M. HAMILL, 2002: Ensemble data assimilation without perturbed observations. – Mon. Wea. Rev. **130**, 1913–1924.

WMO/UNEP, 2010: Scientific Assessment of Ozone Depletion. – Geneva.